Preferred citation: V. Koivu, M. Decain, C. Geindreau, K. Mattila, J. Alaraudanjoki, J.-F. Bloch and M. Kataja. Flow permeability of fibrous porous materials. Micro-tomography and numerical simulations. In **Advances in Pulp and Paper Research, Oxford 2009**, ***Trans. of the XIVth Fund. Res. Symp. Oxford, 2009***, (S.J. I'Anson, ed.), pp 437–454, FRC, Manchester, 2018. DOI: 10.15376/frc.2009.1.437.

FLOW PERMEABILITY OF FIBROUS POROUS MATERIALS. MICRO-TOMOGRAPHY AND NUMERICAL SIMULATIONS

Viivi Koivu[1], Maxime Decain[2,3], Christian Geindreau[3], Keijo Mattila[1], Jarno Alaraudanjoki[1], Jean-Francis Bloch[2] and Markku Kataja[1]

[1] University of Jyväskylä, Department of Physics, BO-Box 35, FI-40014 Jyväskylä, Finland
[2] Papermaking Process Laboratory of Grenoble, 461 rue de la papeterie, BP65, 38402 St Martin D'Heres, France
[3] Laboratory 3S-R, University of Grenoble-CNRS, Domaine Universitaire, BP53, 38041 Grenoble, Cedex 9

ABSTRACT

In this work we demonstrate the use of computerized x-ray micro-tomography and numerical simulations in evaluating flow permeability of fibrous porous materials. This *ab-initio* approach involves solving fluid flow through material samples in the actual pore space obtained by tomographic techniques. The procedure is applied here in three different materials, namely plastic non-woven felt, newsprint and wet pressing felt. All numerical results presented are compared with experimental data for the same materials. The non-woven felt material, having a relatively simple structure, is first used as a test case for comparing two different numerical schemes, lattice-Boltzmann method and a finite-difference method. Here, values of both transverse and in-plane permeability are obtained. The transverse permeability of news-print and wet pressing felt under varying degree of compression is

then found using lattice-Boltzmann method. Finally, we apply the same approach in estimating permeability in different structural layers of the wet press felt material. These material parameters are laborious or even unfeasible to determine experimentally. The procedure is applicable *e.g.* in finding the relevant material parameters for macroscopic models describing calandering, drying and wet pressing processes.

INTRODUCTION

An important problem in analysing and modelling many complex processes found in the industry and nature is to determine realistic material laws that would properly represent *e.g.* the transport properties of materials involved. An essential factor affecting those properties for heterogeneous materials, is their specific internal micro-scale structure. That structure is often very complex and difficult to characterize in a manner that would be readily useful in finding correlations between structural and transport properties of these materials. X-ray microtomography is a relatively new but effective tool for revealing the intrinsic 3D micro-structure of many types of heterogeneous materials [1–6]. Combined with numerical methods, this structure information can be used to find the effective transport properties of such materials [7–11].

Permeability coefficient $\overleftrightarrow{k}$, as defined by Darcys's law [12,13]

$$\vec{q} = -\frac{1}{\mu}\vec{k} \cdot \nabla \psi, \tag{1}$$

for creeping flow through a porous material is a measure of the ability of the material to transmit fluids. Here $\overrightarrow{q}$ is the (superficial) volume flux and μ is the dynamic viscosity of the fluid. The piezometric head ψ is defined by $\nabla\psi = \nabla p - \rho\overrightarrow{g}$ where p is the pressure and ρ is the density of the fluid, and $\overrightarrow{g}$ is the acceleration due to a body force (gravity). Generally, $\overrightarrow{k}$ is a tensor valued quantity. In what follows, we apply Eqn. (1) in cases where $-\nabla\psi$ is in the direction of mean flow that takes place in the three mutually perpendicular coordinate directions (see below). In this case, Eqn. (1) is reduced in a form

$$q_i = -\frac{k_{ii}}{\mu}\frac{\partial \psi}{\partial x_i}, \quad i = 1,2,3 \tag{2}$$

where k_{ii}'s are the diagonal components of the permeability tensor. Experimental values of coefficients k_{ii} are usually determined using an integrated form of Eqn. (2), namely

$$k_{ii} = -\frac{\mu q_i}{(\Delta\psi / \Delta x_i)}, \quad i = 1,2,3 \tag{3}$$

where $\Delta\psi$ is the measured piezometric head difference over a finite distance Δx_i.

A number of theoretical and experimental correlation formulas have been derived that relate the components of permeability coefficient with various structural properties of the porous medium [13,14].

In this work, we demonstrate the approach combining computerized x-ray micro-tomography with direct numerical simulations in evaluating the values of flow permeability coefficient of porous fibrous materials. We start by considering the transverse and in-plane permeability of a plastic non-woven felt having a relatively simple structure. Here, we use two numerical methods, lattice-Boltzmann method and finite-difference method, and compare the results with experimental data for the same material. Next, the approach is applied in finding the dependence of transverse flow permeability on the degree of compression (porosity) for newsprint and wet pressing felt. Also in these cases, the numerical results are compared with experimental data obtained for the same materials. Finally, we utilize the tomographic information on the layered structure of press felt and find the permeability coefficient separately for the top, middle and bottom layers of the felt. The motivation is to demonstrate the potential of the computational approach in obtaining detailed information which is difficult to obtain *e.g.* by direct experiments.

METHODS

In this section we briefly introduce the various methods used in this work, namely x-ray microtomography, finite difference and lattice-Boltzmann methods for solving fluid flow, and an experimental method for measuring transverse as well as in-plane permeability of soft porous materials under mechanical compression.

Tomography and 3D image processing

Computerised x-ray microtomography (CXμT) is a non-intrusive method for 3D imaging of heterogeneous materials with micrometer or sub-micrometer resolution. The method is based on taking a large number (typically, of the

order of 10^3) of x-ray images (shadowgraphs) of the object from different directions. These 2D images are then used to reconstruct the 3D structure of the object using a computational inversion algorithm. Both synchrotron based x-ray beams and conventional x-ray tubes are used as the radiation source. The adequate resolution and the overall quality of the images depends on the techniques used. In this work, both a table-top scanner (Sky-Scan 1172) based on x-ray tube, and a tomographic imaging facility ID19 of the European Synchrotron Radiation Facility (ESRF) were used. The resolution (detail detectability) of the table-top device can be varied from a few micrometers up to few tens of micrometers. With the set-up used at ID19 facility, the resolution was fixed to 0.7 μm.

The tomographic images of material samples were used as a uniform (cubic) grid for numerical solution of flow through the pore space of each sample. To this end, subsections of appropriate size were first cropped out of the original image and filtered by variance-weighted mean filter [15]. Examples of subsections of the original 3D tomographic images for each material type together with the used coordinate convention are shown in Fig. 2 below. The filtered images were thresholded to yield a binary image where the sample volume is divided into solid material and pore space. The three material types were filtered and binarized similarly by selecting the threshold value within the region where the resulting porosity is least sensitive to the threshold value.

Numerical methods for flow solution

The Finite-Difference Method (FDM) implemented in Geodict software [16] was used in this work as a reference numerical method in the case of non-woven felt sample and with selected press felt samples. The diagonal elements of permeability tensor $\overleftrightarrow{k}$ were obtained within FDM by first solving over a periodic representative elementary volume (REV) the following boundary value problem arising from the homogenization process:

$$\begin{aligned} &\mu\Delta\vec{\mathrm{v}} - \nabla p + \rho\vec{g} = 0, && \text{in } \Omega_f \\ &\nabla\cdot\vec{\mathrm{v}} = 0 && \text{in } \Omega_f \\ &\vec{\mathrm{v}} = 0 && \text{on } \Gamma \end{aligned} \tag{4}$$

where Ω_f and Γ represent the fluid volume and the fluid-solid interface, respectively. These three equations are the conservation of momentum, conservation of mass and the no-slip condition on the fluid-solid interface. Here $\vec{\mathrm{v}}$ stands for the periodic microscopic velocity field, p is the first order

periodic fluctuation of the pressure and $\rho\vec{g}$ is the body force. The velocity $\vec{v}$ and the pressure p are discretized on a staggered grid: velocities are defined on their respective voxel faces and the pressure is defined in the centre of the voxel. Then the partial differential equations are solved by using the "*FFF-Stokes solver*" based on Fast Fourier Transform. This solver appears to be fast and memory efficient for large computations dedicated to 3D images [17]. It is used directly on the voxel model without further need for meshing. Due to the staggered grid, if narrow channels (a few voxels) are present, an overestimation of the microscopic velocity, *i.e.* an overestimation of the permeability is generally obtained.

The Lattice-Boltzmann Method (LBM) is based on solving the discrete Boltzmann equation. This can be shown to yield the solutions of the Navier-Stokes equations in the continuum limit [18]. The standard LBM involves an explicit time iteration scheme with a constant time step, uniform grid and local data dependencies. It is ideal for parallel computing. LBM is particularly well suited for solving fluid flow in porous heterogeneous media due to the straightforward implementation of the no-slip boundary condition on fluid-solid interface [18–23]. Here, we use the standard halfway bounce-back boundary condition. Furthermore, we use the particular D3Q19 implementation of LBM with the linear two relaxation time approximation of the Boltzmann equation introduced recently by Ginzburg *et al.* [24]. It appears that this approach avoids the problem of dependence of permeability on viscosity that is encountered within more simple models such as the single relaxation time BKG model [25,26].

The both numerical approaches are well established and also increasingly implemented in commercial softwares. Implementations of the methods are both rather straightforward; however, the FDM being slightly more multi-element. Moreover, the computational times and memory demands for both the methods are nearly the same.

In the present approach the detailed flow solution obtained by FDM or LBM are used to find the numerical estimates for the components of the permeability coefficient using Eqn. (3). Here, the flux q_i is given by the computed total volumetric flow rate in direction x_i divided by total cross sectional area of the sample for a given body force $\rho g_i = (\Delta\psi / \Delta x_i)$ and viscosity μ. The computed values of permeability are, in principle, independent on the selected values of body force and viscosity as long as the resulting flow is well in the creeping flow regime.

Experimental method for permeability measurement

In order to validate the numerical results, the permeability coefficient of the three fibrous materials was measured experimentally using the permeability measurement device (PMD) presented in ref. [27]. That original device can be used to measure the transverse permeability of soft porous sheet-like samples under compression, and using both liquids and gases as permeating fluids. For the purpose of this work the device was modified such that also in-plane permeability can be measured. In transverse flow measurement, a circular sample of diameter 90 mm is placed between smooth sintered stainless steel plates of the same diameter. The peripheral annulus of the sintered plates is blocked leaving a central area of diameter 60 mm open for flow. In the case of in-plane measurements a rectangular sample of size 70 mm × 5 mm, is attached between smooth stainless steel plates and sealed using double sided tapes and elastic sealing compound to avoid flow around the sample and to minimize contact boundary effects (see Fig. 1).

During the measurements the samples were compressed to approximately the same thickness (porosity), or the same range of thickness as the corresponding samples scanned by x-ray tomography (see below). Experiments were conducted with air flow in order to prevent structural changes due to swelling of fibres. This is important in order to obtain similar structure of materials in experiments and in numerical flow solution based on the pore geometry given by tomographic images of dry material samples. Measurements were repeated for five macroscopically identical samples in order to obtain an estimate of the statistical uncertainty of the results.

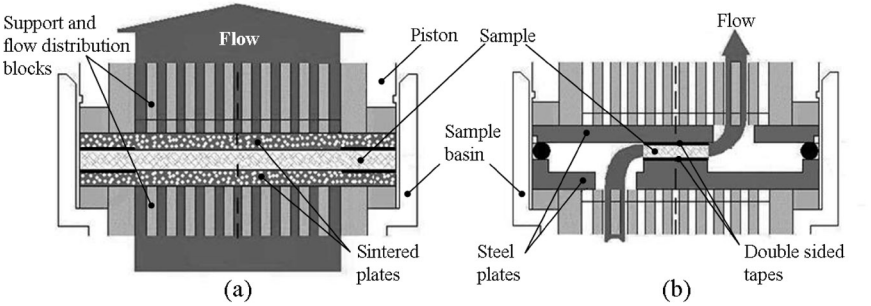

Figure 1. A schematic illustration of the permeability cell and measuring principle used in the PMD apparatus [27] for transverse (a) and in-plane (b) flow directions.

MATERIALS

Three fibrous porous materials with different characteristics were studied. As a first test case of the present method we use a plastic non-woven felt used *e.g* in sound insulating purposes. The internal structure of this material is relatively simple. It is macroscopically quite uniform, isotropic in the in-plane directions and not notably layered in the transverse direction. It is made of plastic fibres with smooth surface and nearly uniform circular cross-section. The structure of newsprint and the shape of individual mechanically pulped wood fibres are clearly more complicated. Wood fibres typically include a lumen and a cell wall with flattened irregular cross section. The fibres are strongly oriented towards the plane of paper and may have preferred orientation within that plane. The conventional wet pressing felt studied here consists of a woven base structure made plastic yarn and needled top and bottom layers of plastic fine batt. The structure of pressing felt is thus anisotropic and less homogeneous than the sound-insulating felt. All these materials are, however, heterogeneous within length scales smaller than a few millimetres. Basic properties of these three fibrous materials are given in Table I. Here, porosity and diameter of fibres are found from binarized 3D tomographic images. The representative fibre diameter was determined as the mean value of the diameters of maximal spheres filling the fibre space in such an image.

The tomographic images of the two types of felts used in this work were obtained using a table-top tomographic scanner at resolution 4.84 μm which appears sufficient for revealing the structural properties of these plastic materials. The newsprint sample was scanned at ESRF at resolution 0.7 μm. Newsprint contains high level of fines which tend to agglomerate and adhere to fibres. Fines can be distinguished from tomographic reconstructions if the size of agglomeration exceeds the resolution of the image. Virtually the fines are detectable in these tomographic reconstructions. When the total volume of the solid phase of the newsprint image is multiplied by a reasonable approximation for wood fibre density, 1200 g/m^3 [28], one receives nearly the experimentally determined basis weight of the sample, see Table I.

The diameter of the samples scanned was 6 mm and 1.4 mm for the two felts and the newsprint samples, respectively. A specific plastic sample holder was used that allows scanning of samples under adjustable static compression in the transverse direction. Visualization of (subsections of) tomographic images of the three materials are shown in Fig. 2 together with the coordinate convention used. For the pressing felt, x direction corresponds to the 'machine direction'. For the newsprint sample, machine direction is not known. The image dimensions (N_x x N_y x N_z) given in the figure caption of

Table I. Some characteristic properties of the materials studied. For pressing felt, the diameters of both the thick base yarn and the fine surface batt are given.

Character	*Sound-insulation felt*	*Newsprint*	*Press felt*
Material	Plastic	Mechanical pulp	Plastic
Basis weight [g/m2]	420 ± 20	52.0 ± 0.5	1630 ± 20
Uncompressed thickness [mm]	1.34 ± 0.01	0.098 ± 0.009	2.44 ± 0.01
Uncompressed porosity [%]	62 ± 1	55 ± 1	42 ± 1
Representative fibre diameter [μm]	34 ± 1	20 ± 1	190 ± 5 / 39 ± 5

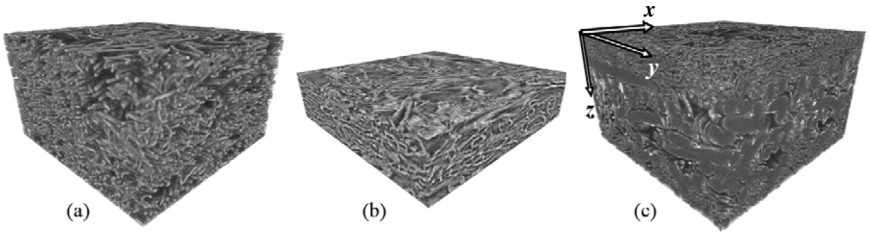

Figure 2. 3D visualization of subsamples of (a) plastic sound-insulation felt, (b) newsprint and (c) plastic wet pressing felt. The grid dimensions of the subsamples are (400 × 400 × 277), (300 × 300 × 121) and (500 × 500 × 490), respectively. The physical dimensions can be obtained by multiplying these dimensions by imaging resolution which is 4.48μm for the two felts and 0.7μm for the newsprint. Also shown in Fig. (c) is the coordinate convention used.

Fig. 2 also give the size of the computational grid used in the numerical solution of fluid flow through these samples.

RESULTS

Before applying the method discussed above in more complicated materials, we aim to test the applicability of the selected numerical schemes and to evaluate the overall accuracy of the method using a fibrous material with relatively simple (but random) structure. Comparison of corresponding numerical and analytical results for regular periodic structures has been reported for example in Ref. [11]. To this end, we first find the transverse and

in-plane permeability of a plastic non-woven sound-insulation felt using the two numerical methods, FDM and LBM, and compare the results with experimental data for the same material. The felt samples scanned by the table-top tomographic device and the samples measured using the PMD were both slightly compressed in the transverse direction such that their thickness was the same in both measurements (within the accuracy of approximately ±15 μm). The numerical and experimental results are summarized in Table II. Here, the transverse permeability $k^{\perp}$ is for mean flow in the z direction and the in-plane permeability is given as the mean value of results computed/measured in x and y directions (see Fig. 2 c). The numerical results obtained by LBM are given as mean values of results from five non-overlapping subsamples, and the experimental results as mean values of five independent measurements. The FDM results given are based on a single subsample.

The largest deviation between the numerical and experimental values is found to be less than 20 % in this case. This is to be compared with the several orders of magnitude variations found in the values of permeability constant between different fibrous materials and even within a single material *e.g.* under different states of compression. The agreement between numerical and experimental values of permeability coefficients is thus found to be very good in this particular case.

We next turn to results from evaluating the dependence on the degree of compression (porosity) of the transverse permeability of newsprint and pressing felt. In this case, individual samples were scanned using the synchrotron facility (newsprint) or the table-top scanner (felt) several times varying their degree of compression between the scans (see Fig. 5). The 3D images thus obtained were processed as discussed above and used as the computational grid for numerical solution of flow by LBM. The transverse permeability of the same materials was also measured using PMD within the same range of degree of compression as used in tomographic imaging.

Table II. Numerical and experimental values of transverse and in-plane permeability for plastic sound-insulation felt. Also given is the statistical uncertainty of LBM and experimental results estimated as the standard deviation of five independent computations/experiments.

Method	$k^{\perp}$ $[10^{-11}\ m^2]$	$k^{\parallel}$ $[10^{-11}\ m^2]$
FDM	3.05	3.42
LBM	2.70 ± 0.30	2.90 ± 0.30
Experimental	2.70 ± 0.05	3.11 ± 0.09

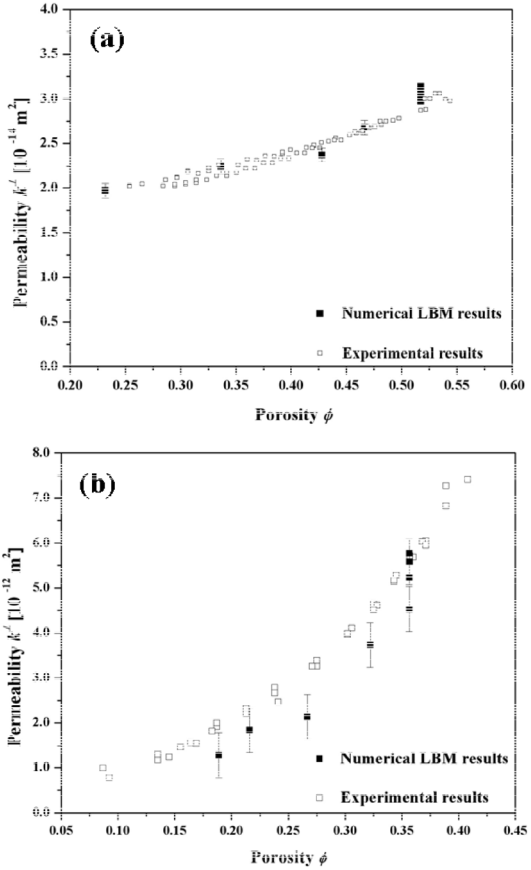

Figure 3. Numerical (LBM) and experimental results for transverse permeability coefficient of newsprint **(a)** and pressing felt **(b)**. The statistical error shown for numerical results is the standard deviation of four analyzed subvolumes. The uncertainty of the experimental results is estimated to be 30 % [27].

Figure 3 shows the computed and measured values of transverse permeability coefficient as a function of porosity. Here, the value of porosity ϕ for the numerical results is obtained by a straightforward analysis of the binarized tomographic images. For the experimental results it is evaluated using the equation

$$\phi \approx 1 - \frac{(1-\phi_0)h_0}{h}, \tag{5}$$

where h is the measured thickness of the sample, and ϕ_0 and h_0 are the porosity and thickness obtained from a tomographic image of the same sample in an arbitrary reference state. This equation is based on the result that the volume of the solid phase remains approximately constant in compression, a result obtained by analysing the tomographic images of the samples at varying degree of compression. The statistical uncertainty of the numerical results for newsprint indicated in Fig. 3 was estimated by repeating the solution for several subvolumes cropped from different locations of the original tomographic image for the highest porosity value. Also in this case the agreement between the measured and numerical results is very good both regarding the order of magnitude of the transverse permeability coefficient and its variation with porosity.

The measured values of transverse permeability coefficient given above were found from Eqn. (3) using the total pressure difference over the entire thickness of the sample. These results (and the corresponding numerical values) thus represent some 'effective' mean values over the transverse dimension of the materials. As discussed above, the structure of the pressing felt is layered, and the properties of the top and bottom layers may differ considerably from those of the middle layer. It is thus unclear, whether such effective mean values are actually useful if applied *e.g.* in modelling wet pressing [29,30,31]. In wet pressing a paper web is compressed against the top layer of the felt, and the typical thickness of that layer is much larger than the thickness of the web. It thus appears that a proper description of fluid flow from the web into the felt requires knowing the properties of various layers of the felt separately and especially, the properties of the top layer next to the paper web. While a direct measurement of *e.g.* permeability of various layers of a pressing felt might be quite tedious, the present method based on tomographic imaging and numerical flow solution provides a straightforward means for such evaluation.

The regions of different kinds of fibres in the triple-layered structure of the pressing felt overlap; the concept of a 'layer' is a matter of definition. Here, we define the layers by means of the distribution of average fibre diameter in the transverse direction. Figure 4 shows such distributions found by the maximal sphere filling algorithm applied on the solid phase in binarized tomographic images of the sample scanned at two levels of compression. The middle layer is clearly visible as a plateau of relatively high values of mean diameter. The positions of the boundaries between the layers are defined as locations where the average fibre diameter has the value half-way between the typical values at the middle and surface layers. The same criterion for the layers is used for all states of compression. It was verified by visual inspection, that the layers specified in this manner indeed include closely the same

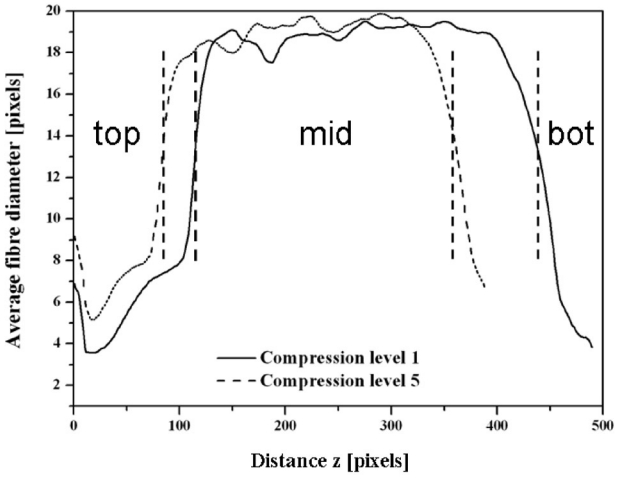

Figure 4. Distribution of mean fibre diameter in transverse direction in two states of compression of the pressing felt sample. The vertical dashed lines indicate positions of boundaries between the top (paper side), middle and bottom (roll side) layers of the felt.

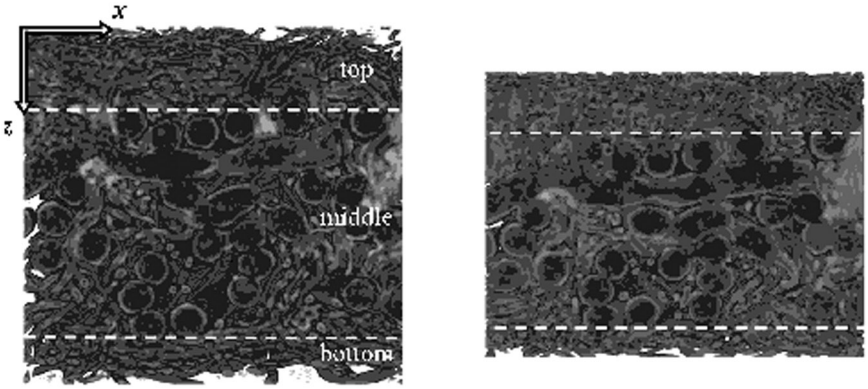

Figure 5. 2D slices of tomographic images of the wet pressing felt sample in two different states of compression. Also shown are the top, middle and bottom layers as specified in Fig. 4.

fibre material points in tomographic images corresponding to different levels of compression. It thus seems justified to compare the results obtained for each individual layer under varying degree of compression.

The numerically computed dependence on compression (thickness of the entire felt sample) of transverse and in-plane permeability coefficients for the three layers of pressing felt are shown in Fig. 6. In Fig. 7 shown is the same data but plotted for each layer as a function of porosity of that layer. Computations have been made using LBM for several subsamples in the cases of the highest porosity values and for a single subsample in all other cases. Also shown are the results for the in-plane permeability obtained by FDM for the highest values of porosity. The transverse permeability of the top layer is, as

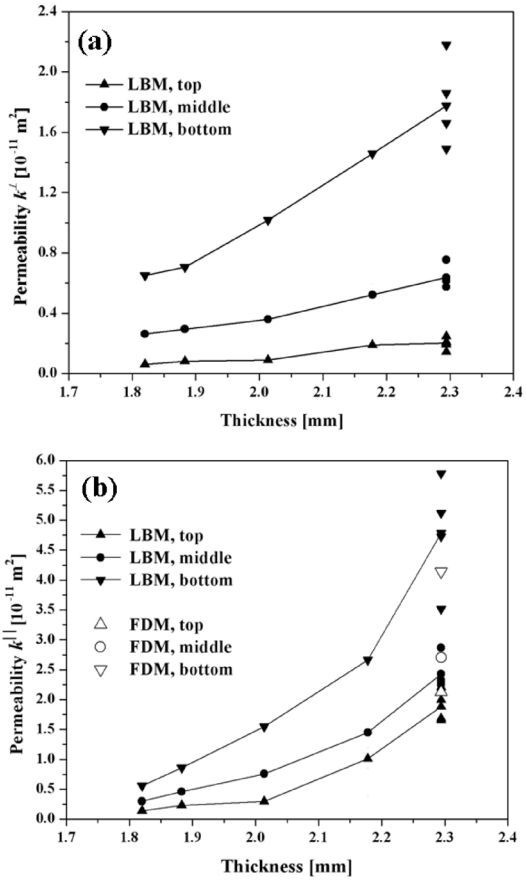

Figure 6. Numerical values of transverse (a) and in-plane (b) permeability coefficient for top, middle and bottom layers of the pressing felt as a function of thickness of the entire sample.

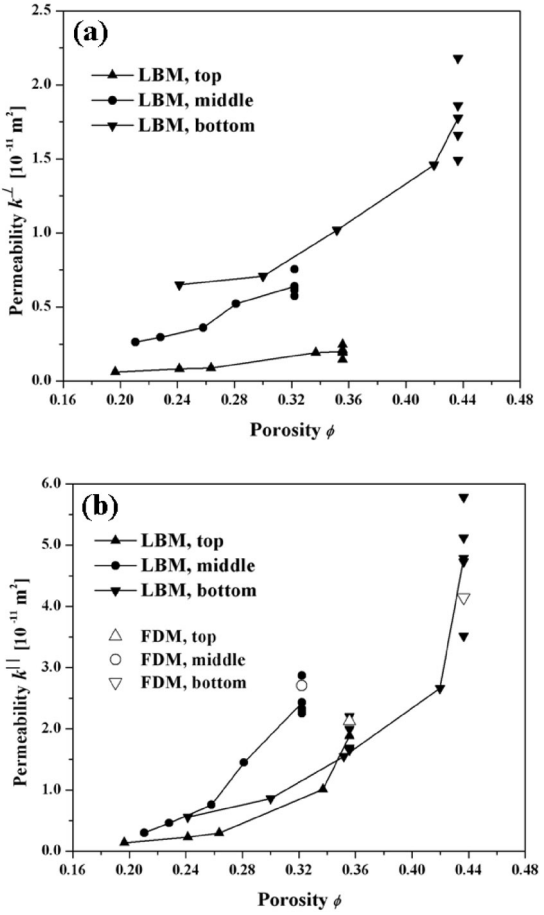

Figure 7. Same as Fig. 6, but the data for each layer plotted as a function of porosity. That is, the porosity is measured separately for each layer.

expected, lower than the permeability of the middle layer. This is simply due to higher specific surface of the fine batt fibres in the top layer. Instead, the transverse permeability of the bottom layer at a given degree of compression is much higher than that of the top and middle layers. This is explained partly by the higher porosity of the bottom layer, as shown by Fig. 7 (a), and partly by the fact that the bottom layer is very thin. Obviously, it includes open flow channels through the entire layer. This results in a lower value of flow resistance than that of a corresponding bulk material. Instead, as shown by Fig. 7

(b), the in-plane permeability of the top and bottom layers fall approximately on the same curve when plotted as a function of porosity. This is as expected since the radius, and thus the specific surface of fibres in these surface layers is nearly the same (and there is no channelling effect present in the lateral flow direction).

Comparing the results shown in Fig. 3 (b) and Fig. 6 (a) indicates that the behaviour of the mean transverse permeability differs significantly from that of individual layers. For the present pressing felt sample, the transverse permeability of the top layer is smaller than the mean transverse permeability by a factor of 2–3 in the range of overall compression studied here. Similar result is valid also for the in-plane permeability. Clearly, such a difference should be taken into account *e.g.* in numerical analysis of water removal in wet pressing. Notice however, that the results shown in Figs. 6 and 7 are for a room-dry sample of pressing felt, and given here in the purpose of demonstrating the use of the present techniques. In order to obtain results appropriate for actual wet pressing applications the analysis should be repeated for wet and swollen felt samples. That analysis is left for a future work.

CONCLUSIONS

Experimental approach is often considered as the only practical means for finding the macroscopic transport properties of heterogeneous materials. Even in the case that the basic transport dynamics is well known, the complex and irregular microstructure of those materials, unknown in general, may render analytical or numerical approaches based on averaged or statistical methods ineffective or inaccurate. Combining x-ray micro-tomography with numerical methods can provide new possibilities in finding transport properties of heterogeneous materials such as paper and paper-making fabrics. Within this *ab-initio* approach detailed structural information obtained by micro-tomography is used as input to numerical solver to find the necessary macroscopic transport properties by means of direct numerical simulation in the micro scale.

In this work we demonstrated the applicability of this procedure in finding the Darcian flow permeability coefficients for three different fibrous materials. The method was first validated for a non-woven plastic felt material with rather simple (but random) structure. The internal microstructure of this material was found using a table-top tomographic scanner. The values of the transverse and in-plane permeability coefficients were then found using two conceptually different numerical methods, finite difference method and lattice-Boltzmann method. The results were compared with

experimental values of permeability measured for air flow through the same material. The maximum deviation between numerical and experimental results was less than 20 %. The procedure was then applied in evaluating the behaviour of transverse permeability of newsprint and pressing felt under mechanical compression. Here, the structure of the pressing felt sample was again obtained by a table-top tomographic device, while the paper sample was scanned at the ID19 laboratory of the European Synchrotron Radiation Facility, both under varying degrees of compression. The numerical results were obtained by the lattice-Boltzmann method and the results were compared with the corresponding experimental results. The agreement between experimental and numerical results was again found to be very good for these two materials regarding both the absolute value of the transverse permeability coefficient and its dependence on the degree of compression.

Finally, the same procedure was applied in evaluating the dependence on degree of compression of transverse and in-plane permeability – separately for top, middle and bottom layers of the pressing felt. This application demonstrates the potential of the present method in obtaining such detailed and new information on material properties that would be very difficult to obtain *e.g.* by direct experiments.

ACKNOWLEDGEMENTS

Authors thank staff members of the workshop of University of Jyväskylä for the technical work related to modifications of the PMD. Also productive discussions with M.Sc. Tuomas Turpeinen during preparation of this article are gratefully acknowledged.

REFERENCES

1. E. J. Samuelsen, P.-J. Houen, O. W. Gregersen, T. Helle and C. Raven. Three Dimensional Imaging of Paper by Use of Synchrotron X-ray Microtomography, *J. Pulp and Paper Sci.* **27**(2):50–53, 2001.
2. A. Goel, M. Tzanakakis, S. Huang, S. Ramaswamy, D. Choi, and B. Ramarao. Characterization of three-dimensional structure of paper using Xray microtomography. *Tappi J.* **84**(5):111–122, 2002.
3. X. Thibault and J.-F. Bloch, J.-F. Structural Analysis of X-ray Microtomography of a Strained Nonwoven Papermaker Felt. *Textile Research Journal*, **72**(6), 480–485, 2002
4. R. Holmstad, C. Antonie, P. Nygård and T. Helle. Quantification of the three-

dimensional paper structure: Methods and potential. *Pulp & Paper Canada*. **42**(7):186–189, 2003.
5. S. Rolland du Roscoat, J.-F. Bloch and X. Thibault. Synchrotron Radiation microtomography applied to paper investigation. *Journal of Physics D: Applied Physics*, 38: A78–A84, 2005.
6. A. Goel, C. H. Arns, R. Holmstad, O. W. Gregersen, F. Bauget, H. Averdunk, R. M. Sok, A. P. Sheppard and M. A. Knackstedt. Analysis of the Impact of Papermaking Variables on the Structure and Transport Properties of Paper Samples by X-ray Microtomography, *J. Pulp and Paper Sci.* **32**(2):111–122, 2006.
7. N.S. Martys and J.G. Hagedorn. Multiscale modeling of fluid transport in heterogeneous materials using discrete Boltzmann methods. *Journal of Materials and Structures*, **35**(10):650, 2002.
8. U. Aaltosalmi, M. Kataja, A. Koponen, J. Timonen, A. Goel, G. Lee and S. Ramaswamy. Numerical Analysis of Fluif Flow Through Fibrous Porous Materials. *Journal of Pulp and Paper Sience*. **30**(9):251–255, 2004.
9. S. Ramaswamy, M. Gupta, A. Goel, U. Aaltosalmi, M. Kataja, A. Koponen and B. V. Ramarao. The 3D structure of fabric and its relationship to liquid and vapor transport. *Colloids and Surfaces A: Physicochem. Eng. Aspects*, 241: 323–333, 2004.
10. W. Fourie, R. Said, P. Young and D. L Barnes. The simulation of pore Scale Fluid Flow with Real World Geometries Obtained from X-Ray Computed Tomography. *European COMSOL Multiphysics Conference, Boston*. COMSOL inc., 2007.
11. V. Koivu, M. Decain, C., Geindreau, K., Mattila, J.-F. Bloch and M. Kataja. Transport Properties of Heterogeneous Material Combining Computerized X-ray Micro-Tomography and Direct Numerical Simulations. Submitted to *International Journal of Computational Fluid Dynamics*, 2009.
12. H. Darcy. Les Fontaines Publiques de la Ville de Dijon, Paris, 1856.
13. J. Bear. Dynamics of Fluid in Porous Media. Dover Publications inc, New York, pp.151–173, 1972.
14. G. W. Jackson and D. F. James, 1986. The Permeability of Fibrous Porous Media, *Can. J. Chem. Eng.* 64, 364–373
15. R. C. Gonzales and R. E Woods. Digital Image Processing, Prentice-Hall Inc. New Jersey, second edition, pp. 237–241, 2001.
16. Geodict website, www.geodict.com, accessed 10.9.2008.
17. A. Wiegman. Computation of the permeability of porous materials from their microstructure by FFTStokes. Report of the Fraunhofer ITWM, 129, 2007.
18. S. Succi. The Lattice Boltzmann Equation: For Fluid Dynamics and Beyond. Clarendon Press, Oxford, 2001.
19. A. Koponen, D. Kandhai, E. Hellén, M. Alava, A. Hoekstra, M. Kataja, K. Niskanen, P. Sloot and J. Timonen. Permeability of Three-Dimensional Random Fiber Webs. *Physical Review Letters*, **80**(4), 716, 1998.
20. C. Manwart, U. Aaltosalmi, A. Koponen, R. Hilfer and J. Timonen. Lattice-Boltzmann and finite-difference simulations for the permeability for three-dimensional porous media. *Physical. Review E*, **66**(1), 016702, 2002.

21. N.S. Martys and J.G. Hagedorn. Multiscale modeling of fluid transport in heterogeneous materials using discrete Boltzmann methods. *Journal of Materials and Structures*, **35**(10), 650, 2002.
22. M.E. Kutay, A.H. Aydilek, and E. Masad. Laboratory validation of lattice Boltzmann method for modeling pore-scale flow in granular materials. *Computational Geotechnics*, 33, 381–395, 2006.
23. C. Pan, L.-S. Luo and C.T. Miller. An evaluation of lattice Boltzmann schemes for porous medium flow simulation. *Computers & Fluids*, **35**(8–9), 898, 2006.
24. I. Ginzburg, F. Verhaeghe and D. d'Humiéres. Two-Relaxation-time Lattice-Boltzmann scheme: About Parametrization,Velocity, Pressure and Mixed Boundary Conditions. *Communications in Computational Physics*, **3**(2), 427–478, 2008.
25. I. Ginzburg and D. d'Humiéres. Multireflection boundary conditions for lattice Boltzmann models. *Physical Review E*, **68**(6), 066614, 2003.
26. I. Ginzburg. Consistent lattice Boltzmann schemes for the Brinkman model of porous flow and finite Chapman-Enskog expansion. *Phys. Rev. E*, (77):066704, 2008.
27. V. Koivu, K. Mattila and M. Kataja. A Method for Measuring Darcian Flow Permeability of Thin Compressed Fibre Mats. Submitted to *Nordic Pulp and Paper Research Journal*, February 2009.
28. M. Leskelä and S. Simula. Transport Phenomena. Ch. 9 in Paper Physics, Papermaking Science and Technology, book 16 (ed. K Niskanen), Fapet Oy, Jyväskylä, 1998.
29. J. C. Roux and J. P. Vincent, A proposed model in the analysis of wet pressing, *TAPPI J.* 74(2), 189, 1991.
30. F. El-Hosseiny, Mathematical modelling of wet pressing of paper, *Nordic Pulp and Paper Res. J.* 6(1), 30, 1991.
31. M. Kataja, K. Hiltunen and J. Timonen, Flow of water and air in a compressible porous medium. A model of wet pressing of paper, *J. Phys. D: Appl. Phys.* 25, 1992.

FLOW PERMEABILITY OF FIBROUS POROUS MATERIALS. MICRO-TOMOGRAPHY AND NUMERICAL SIMULATIONS

Viivi Koivu,[1] *Maxime Decain*,[2,3] *Christian Geindreau*,[3] *Keijo Mattila*,[1] *Jarno Alaraudanjoki*,[1] *Jean-Francis Bloch*[2] and *Markku Kataja*[1]

[1]University of Jyväskylä, Department of Physics, BO-Box 35, FI-40014 Jyväskylä, Finland
[2]Papermaking Process Laboratory of Grenoble, 461 rue de la papeterie, BP65, 38402 St Martin D'Heres, France
[3]Laboratory 3S-R, University of Grenoble-CNRS, Domaine Universitaire, BP53, 38041 Grenoble, Cedex 9, France

Lars Wågberg KTH

Thank you very much for a clear and very interesting talk. In one of your studies, I think it is second to last slide (figure 7 in the paper in the proceedings, ed.), you showed that at the same porosity you have a very large difference in permeability between the layers. Could you explain this? What is that depending on, is it the orientation of fibres, or distribution of pores, or some other reason?

Viivi Koivu

Yes, I think it comes from the fibre diameter which causes higher specific surface area on the top and bottom layers compared to the middle layer. The diameter of the fibres on the top and bottom layers is slightly different. I think it has something to do with that.

Discussion

Lars Wågberg

Yes, this approach definitely opens up new dimensions for network optimization. It is a new tool for optimizing structures and orientations and selecting new parameters. Very interesting. Thank you.

Kit Dodson University of Manchester

These are really fascinating results. Could we look at the slide for the newsprint sample (figure 3a in the paper in the proceedings, ed.)? The remarkable thing here – if we go back to the table – you have a table of the values in-plane and perpendicular for the newsprint, am I right, this is for the newsprint?

Viivi Koivu

No, the results are for the non-woven felt.

Kit Dodson

Do we have this data for the newsprint in a table?

Viivi Koivu

No, I am sorry.

Kit Dodson

Okay! Then, it is the next slide (Table II in the paper in the proceedings, ed.). So from that table, there is very little difference between the in-plane and perpendicular. Now in the case of the newsprint, we have definitely a layered structure. We have probably 10 layers of fibres in a sense, we have got something like 10 fibres deep, so we would expect the difference. Do we have a difference detected?

Viivi Koivu

Yes, definitely, there is a difference; but it was not included into this work. The factor is from 2 to something like 6.

Kit Dodson

Yes, thank you.

Jean-Claude Roux University of Grenoble

In your experiments on the wet press felt, am I correct if I say that when I increase the compression, I will reduce the difference between permeability of the top and bottom surfaces?

Viivi Koivu

Yes.

Jean-Claude Roux

Thank you.

Ilya Vadeika FPInnovations

Again following on the questions about the felts. Felts often have treatments on the top and the bottom is not treated. The treatment varies depending on the felt, the batt fibres can be heat treated or chemically treated to change the structure of the top side of the felt. In your case, was the top side of the felt treated or not?

Viivi Koivu

This particular press felt is very old, so I think there is no treatment. Actually, I do not know.

Ilya Vadeika

Okay, but the fibres themselves of the batt on the top and the bottom, are these the same or different?

Viivi Koivu

They are a slightly different.

Ilya Vadeika

Thank you.

Discussion

Shri Ramaswamy University of Minnesota

In your numerical method, how do you compute the permeability when you are looking at the individual layers: top, middle, and bottom? Do you actually compute the flow velocity and pressure loss for each section?

Viivi Koivu

We calculate flow velocity and pressure loss, and by Darcy's law we calculate the permeability.

Shri Ramaswamy

And that is for the whole sample and you do the same thing for the individual sections?

Viivi Koivu

Yes, thank you for the question.

Ramin Farnood University of Toronto.

I assume that the purpose of this type of study is to look into the press section. During the pressing operation, there is a transient behaviour where we have drainage and, at the same time, there is a compression of the web. Can you comment on the applicability of parameters which you are using in your model to this transient process? And have you examined if the Darcy's coefficient that you are extracting would be valid for a rapid compression in the press nip?

Viivi Koivu

I have to admit that I am not a specialist on those rapid measurements or rapid phenomena. So I think, I cannot answer that question; but anyways these results can be used to model press section, somehow, hopefully, one day!

Wolfgang Bauer Graz University of Technology

In paper you also have capillary flow, can you account for that too?

Viivi Koivu

No, we enforce the flow with pressure and we do not take any capillary forces into account. At least, not at the moment.

Tetsu Uesaka FPInnovations

This is a comment. One of my colleagues, David Vidal of FPInnovations, did a similar kind of Lattice-Boltzmann simulation to predict permeability with a coating structure. The coating structure consists of a randomly packed particle system, which is very similar to the one we have in the paper. What he found was that, basically, most of the permeability data fits very well to the conventional Kozeny-Carman equation, with a slight modification. Everything fitted very, very well – disappointingly. So this means that he was very much disappointed by the fact that, what he predicted with all this effort very much fitted to the kind of equations which were developed many, many years ago. So did you find something similar; did you try to organise the data in such a way?

Viivi Koivu

No, and thank you for your question.

Ilya Vadeika FPInnovations

A quick technical question, what was the size of the system that you modelled in-plane.

Viivi Koivu

For the press felt, it was about 2.5 mm × 2.5 mm in real physical dimensions.

Ilya Vadeika

And for the paper?

Viivi Koivu

For the paper, it was of the order of 0.5 mm × 0.5 mm.

Ilya Vadeika

Thank you!